Wind and Structures, *Vol. 20, No. 1 (2015) 15-36*
DOI: http://dx.doi.org/10.12989/was.2015.20.1.015

The appropriate shape of the boundary transition section for a mountain-gorge terrain model in a wind tunnel test

Peng Hu[1a], Yongle Li[*2], Guoqing Huang[2], Rui Kang[3] and Haili Liao[2]

[1]*School of Civil Engineering and Architecture, Changsha University of Science & Technology, Changsha, Hunan 410114, China*
[2]*School of Civil Engineering, Southwest Jiaotong University, Chengdu, Sichuan 610031, China*
[3]*Department of Civil Engineering, Southwest Jiaotong University, Emei, Sichuan 614202, China*

(Received March 14, 2014, Revised September 8, 2014, Accepted November 1, 2014)

Abstract. Characterization of wind flows over a complex terrain, especially mountain-gorge terrain (referred to as the very complex terrain with rolling mountains and deep narrow gorges), is an important issue for design and operation of long-span bridges constructed in this area. In both wind tunnel testing and numerical simulation, a transition section is often used to connect the wind tunnel floor or computational domain bottom and the boundary top of the terrain model in order to generate a smooth flow transition over the edge of the terrain model. Although the transition section plays an important role in simulation of wind field over complex terrain, an appropriate shape needs investigation. In this study, two principles for selecting an appropriate shape of boundary transition section were proposed, and a theoretical curve serving for the mountain-gorge terrain model was derived based on potential flow theory around a circular cylinder. Then a two-dimensional (2-D) simulation was used to compare the flow transition performance between the proposed curved transition section and the traditional ramp transition section in a wind tunnel. Furthermore, the wind velocity field induced by the curved transition section with an equivalent slope of 30° was investigated in detail, and a parameter called the 'velocity stability factor' was defined; an analytical model for predicting the velocity stability factor was also proposed. The results show that the proposed curved transition section has a better flow transition performance compared with the traditional ramp transition section. The proposed analytical model can also adequately predict the velocity stability factor of the wind field.

Keywords: mountain-gorge terrain; boundary transition section; wind characteristics; potential flow; wind tunnel test

1. Introduction

When the wind flows over mountain-gorge terrain (it is referred to as 'very complex terrain' with rolling mountains and deep narrow gorges as shown in Fig. 1), wind is obstructed and deflected by the mountains, and flow separation usually occurs downwind of the mountains. On the other hand, the flow can accelerate or decelerate as it moves through gorges. Therefore, wind

∗Corresponding author, Professor, E-mail: lele@swjtu.edu.cn
[a] Ph.D., E-mail: hupengmail@126.com

http://www.techno-press.org/?journal=was&subpage=8 ISSN: 1226-6116 (Print), 1598-6225 (Online)

characteristics over the mountain-gorge terrain are extremely complicated. Many researchers have investigated the wind characteristics over such complex terrains and found they are important not only for wind energy, pollution dispersion and forest fires (Maurizi *et al*. 1998), but also for the loading of structures (Li *et al*. 2010a). In recent years, several long-span bridges have been built in mountain-gorge terrains, especially in the west regions of China, including the Beipanjiang Great Bridge in Guizhou province and the Siduhe Great Bridge in Hubei province, which are both shown in Fig. 1. If these bridges are designed by current design standards and codes based on flat, homogeneous terrain, the resulting prediction of wind-induced responses may lead to significant errors (Chock and Cochran 2005, Li *et al*. 2010a). Therefore, there is a clear need to better model and characterize the wind flows over these complex terrains.

The determination of wind characteristics over mountain-gorge terrain is difficult. Current theoretical studies mainly focus on smooth and isolated hills, rather than real mountain-gorge terrain (Jackson and Hunt 1975, Mason and Sykes 1979, Hunt *et al*. 1988). Field measurements are expensive to be carried out and easily affected by the environmental conditions (Hui *et al*. 2009). Compared with the theoretical studies and field measurements, wind tunnel testing and numerical simulation by computational fluid dynamics (CFD) have been widely adopted to analyze the wind characteristics over complex terrain (Cao and Tamura 2006, Carpenter and Locke 1999, Kim *et al*. 2000, Loureiro *et al*. 2008) due to the convenience of controlling, and changing the test conditions. Based on wind tunnel testing, Neal *et al*. (1981) investigated the effects of three different forms of model construction, that is terraced, contoured and roughened surfaces, on the wind flow over a complex terrain, and found that the velocity and turbulence intensity profiles produced by the terraced form were significantly different from those from the other two forms, and correction required between the contoured and roughness-added models was as high as 0.94. Meroney (1980) studied the flow over a complex terrain model in a wind tunnel and compared the results with those from the numerical simulation and field measurements. The results indicated that the generation of equivalent wind speeds near ground level requires accurate reproduction of surface roughness, shape and vegetation, and hence a terraced model is not as suitable as a contoured model in such circumstances. Cermak (1984) reviewed the physical techniques of modeling the atmospheric motion in different meteorological conditions, such as the neutral atmospheric boundary layer, stratified atmospheric boundary layer and pure gravitational convection, and pointed out that the oncoming wind flow and local surface details have important effects on the simulation results. Bowen (2003) comprehensively discussed the wind tunnel testing issues relating to the wind flows over a complex terrain, during the neutrally stable, strong wind events, and guidelines for Coriolis force effects, atmospheric stability, aerodynamic roughness, flow turbulence and flow separation were identified, enabling the design of appropriate wind tunnel testing model at relatively small geometric scales. To better understand the wind characteristics over the mountain-gorge terrain, Li *et al*. (2010a) investigated the wind characteristics over representative, simplified valley terrains and existing real valley terrain, and obtained some useful fundamental information by comparing the results obtained from these two types of valley terrain.

However, a wind tunnel cannot well address the geophysical processes of thermal stratification and the effects of Coriolis force. To consider these two issues, a hybrid tool of the wind tunnel test and the numerical simulation methods was developed by Derickson and Peterka (2004), and this hybrid tool was used to evaluate the wind power site in complex terrain. Li *et al*. (2010b) combined a meteorological model and a commercial CFD model as a nested modeling system, which can provide not only realistic boundary conditions containing terrain information on the

upwind direction, but also simulation results with a higher spatial resolution. In addition, it can accurately describe the terrain features in simulation of wind field over complex terrain. On the other hand, if the numerical simulation is used to study the wind characteristics over the complex terrain, the following issues including the turbulence models, boundary conditions and mesh size also need to be carefully considered (Maurizi *et al*. 1998, Iizuka and Kondo 2004), and the results should be compared with those obtained from the wind tunnel test or the field measurements (Derickson and Peterka 2004, Tsang *et al*. 2009).

To model complex terrain, particularly mountain-gorge terrain, in a wind tunnel or in a numerical computational domain, one further challenge will be encountered. Since the terrain domain chosen to be analyzed is always limited, its range is generally determined by truncating the unbounded mountain-gorge terrain at an appropriate distance from the bridge site. As is well known, the mountain-gorge terrain usually is located at a high altitude, and the elevations around the boundary may be significantly different. Hence, a sudden elevation jump (Δh, as shown in Fig. 2) between the boundary top of the terrain model and the wind tunnel floor (or the bottom of the numerical computational domain) will usually exist. Also the jump may vary significantly around the edge of the model of the complex terrain. If the wind flows over this untreated model, flow obstruction and separation will occur over the terrain model edge, producing an unrealistic flow pattern and the significant errors will be introduced. To produce smoother oncoming wind flows at the edge of the terrain model, an elevation transition section from the wind tunnel floor (or the bottom of the numerical computational domain) to the boundary top of the terrain model should be established. Meroney (1980) adopted an additional terrain section to transition the wind tunnel floor to the terrain model. However, the form of the terrain transition section was not provided in detail. Hu *et al*. (2006) employed a ramp-transition section with a slope of 30° to investigate the wind characteristics at a bridge site in mountain-gorge terrain. Based on the numerical simulation method, Maurizi *et al*. (1998) used a ramp-transition section with the maximum slope of 10% to simulate a more realistic oncoming wind field, in order to predict the wind field over mountainous terrain. Although these transition sections help to generate a more realistic wind field in the complex terrain, one problem is not solved: how to determine an appropriate boundary transition section shape, to allow generation of more physically meaningful flows over the terrain boundary.

Because an upstream oncoming wind field is not disturbed by a terrain model located in a wind tunnel (or a numerical computational domain), it can be regarded as a reference wind field. When wind flows over an appropriate boundary transition section, the wind field at the end of the section should maintain the same characteristics as those of the undisturbed reference as much as possible. In order to achieve this target in a wind tunnel test or numerical simulation, the following two principles should be satisfied in designing an appropriate shape of boundary transition section. Firstly, the major wind parameters such as the wind velocity and angle of attack at the end edge of the transition section should be maintained to be the same as those of the reference wind field, when the oncoming wind flows over the transition section. Otherwise, the oncoming wind will be significantly affected by the transition section and may be not meaningful for wind characteristics study. Secondly, the total length of the oncoming wind flowing from the start position of the transition section, to the position where the wind field becomes stable and approaches the undisturbed reference wind field (‘total flow transition length’ for short), should be sufficiently short. Obviously, a longer total flow transition will reduce the model scale as the size of the wind tunnel test section is limited. If a numerical simulation is adopted, a longer total flow transition will enhance the computational cost due to the increase of the computational domain size. Therefore, these two principles will be considered simultaneously if the transition section is

required to have a relatively good flow transition performance.

When the oncoming wind flows over the ramp transition section with a slope of 30° (previously used by Hu *et al*. 2006), the pressure gradient changes from an adverse one to a positive one. As a result, the oncoming wind accelerates and reaches the maximum velocity at the top of the ramp transition section (position *s*, shown in Fig. 3), and a significant speed-up behavior of the oncoming wind occurs. Furthermore, the wind pressure also reaches the minimum value and an adverse pressure gradient develops around the position *s*. In such circumstances, flow separation may occur if the adverse pressure gradient becomes sufficiently large (Hu *et al*. 2012), possibly resulting in a thicker boundary layer and an unstable wind flow. In general, the behavior of speed-up and flow separation around the position *s* are the two main shortcomings for this ramp transition section, and they can cause noticeably different wind characteristics from those of the reference wind. For the ramp transition section with the maximum slope of 10% (previously used by Maurizi *et al*. 1998), although flow separation is unlikely to occur (Kondo *et al*. 2002), and the speed-up behavior of the oncoming wind may be not evident, the longer transition section itself will result in a longer total flow transition length. Hence, the previous two ramp transition sections may be not suitable to transition the wind flow for the wind field simulation in mountain-gorge terrains, and a new type of transition section should be developed to improve the flow transition performance for the wind characteristics study in mountain-gorge terrains.

In this paper, in order to better simulate the wind field over the mountain-gorge terrain, a type of theoretical curve, providing a suitable shape of boundary transition section for mountain-gorge terrain model, was derived based on potential flow theory around a circular cylinder. Then, a 2-D platform terrain model was adopted to investigate the flow transition performance for the curved and the ramp transition sections, using wind tunnel tests. In addition, a curved transition section with an equivalent slope of 30° was specifically studied. A parameter called ‘velocity stability factor’ was defined, and an analytical model for predicting this factor was proposed based on potential flow theory around a blunt nosed semi-infinite streamline body and corresponding test data. Finally, some main conclusions were given.

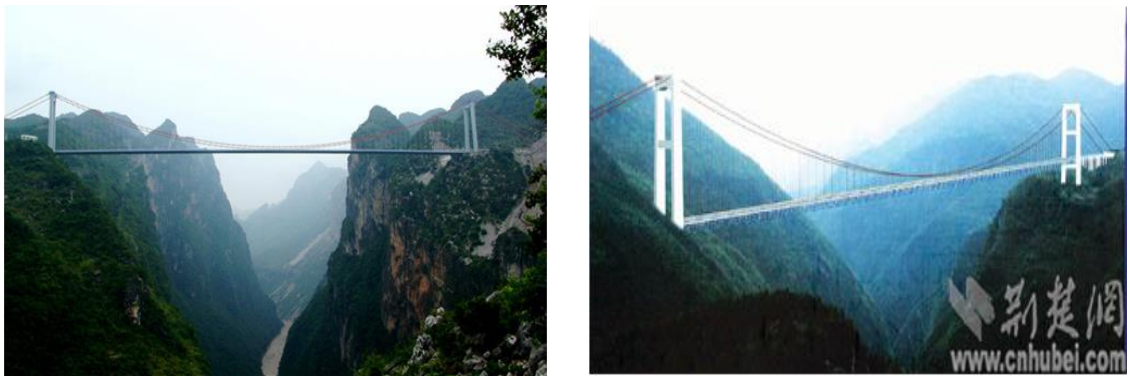

(a) Beipanjiang Great Bridge in Guizhou Province (b) Siduhe Great Bridge in Hubei Province

Fig. 1 Long-span bridges located in the mountain-gorge terrain

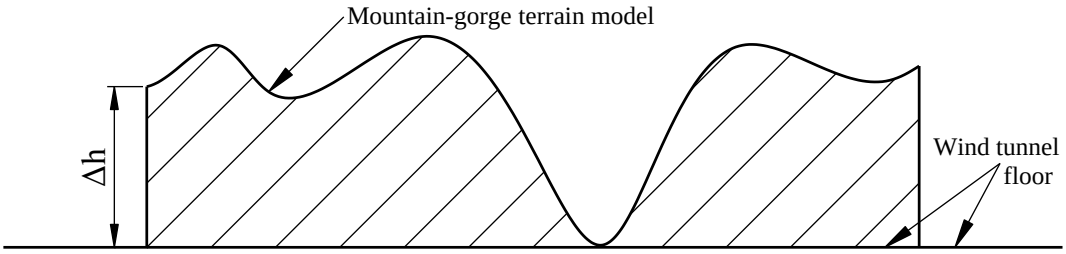

Fig. 2 A sudden elevation jump between the boundary top of the terrain model and the wind tunnel floor

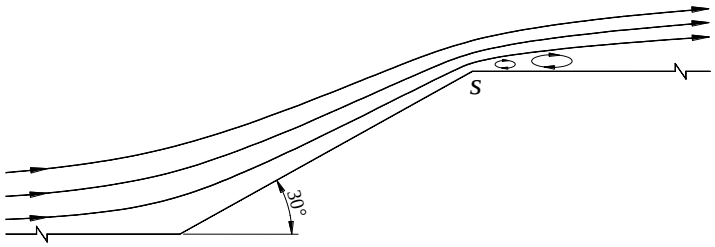

Fig. 3 Oncoming wind flows over a ramp transition section with the slope of 30°

2. Derivation of transition section curves based on potential flow theory around a circular cylinder

Assume that the undisturbed reference wind field is a uniform rectilinear flow and its vertical wind velocity is zero. When the oncoming wind flows over the transition section, except for small regions near the wall of the transition section influenced by viscous effects, the other regions can be considered as potential flow. According to the classic theory of potential flow around a circular cylinder, the stream function and wind velocities are given as follows (Currie 2003)

$$\psi = U_\infty y\left(1-\frac{r^2}{x^2+y^2}\right) \tag{1}$$

$$u = \frac{\partial \psi}{\partial y} = U_\infty\left[1+r^2\frac{y^2-x^2}{\left(x^2+y^2\right)^2}\right] \tag{2}$$

$$v = -\frac{\partial \psi}{\partial x} = -U_\infty r^2\frac{2xy}{\left(x^2+y^2\right)^2} \tag{3}$$

where ψ is the stream function and it is a constant for each streamline; U_∞ is the oncoming wind velocity at infinity; r is the radius of the circular cylinder; u and v are the longitudinal and vertical velocities; x and y are the corresponding coordinates of the flow field, as shown in Fig. 4.

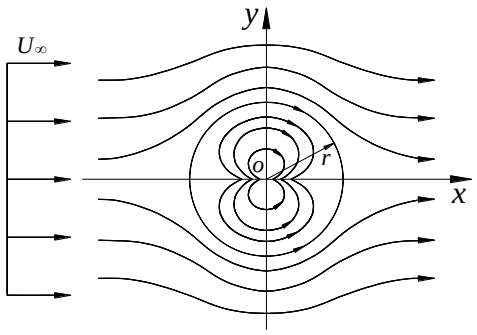

Fig. 4 Potential flow around a circular cylinder

Based on the first principle presented in introduction, the vertical velocity of the oncoming wind should be equal to zero at least at the start and end positions of the transition section. From Eq. (3), it can be seen that the vertical velocity v is equal to zero only when $x = 0$ or $x = \pm\infty$. Furthermore, according to the basic properties of the stream function (Currie 2003), each streamline can be regarded as a wall with no influences on the oncoming wind movements, and the flow separation does not occur when the oncoming wind is flowing along the streamline. Therefore, the streamline can be used as the candidate shape of the boundary transition section, that is, the coordinate points of $x = 0$ and $x = \pm\infty$ on the streamlines are the possible start and end positions for the transition section. However, the transition section would have a limitless length according to the previous discussion. To obtain a meaningful transition section, a new form of the streamline function can be derived from Eq. (1) and given as follows

$$\begin{aligned}\psi &= U_\infty y\left[1-\frac{r^2}{y^2}\cdot\frac{1}{1+(x/y)^2}\right]\\ &= U_\infty y\left[1-\frac{r^2}{y^2}\cdot\sum_{n=0}^{\infty}(-1)^n\left(\frac{x}{y}\right)^{2n}\right]\\ &= U_\infty y\left\{1-\frac{r^2}{y^2}\left[1-\left(\frac{x}{y}\right)^2+\left(\frac{x}{y}\right)^4-\left(\frac{x}{y}\right)^6+\left(\frac{x}{y}\right)^8-\left(\frac{x}{y}\right)^{10}+\cdots\right]\right\}\end{aligned} \tag{4}$$

For better applications in engineering practice, only the first five terms in Eq. (4) should be retained, and the corresponding stream function and the vertical wind velocity are given as

$$\psi_5 = U_\infty y - r^2U_\infty\frac{1}{y}+r^2U_\infty\frac{x^2}{y^3}-r^2U_\infty\frac{x^4}{y^5}+r^2U_\infty\frac{x^6}{y^7}-r^2U_\infty\frac{x^8}{y^9} \tag{5}$$

$$v_5 = -\frac{\partial\psi_5}{\partial x} = -2r^2U_\infty\frac{x}{y^3}+4r^2U_\infty\frac{x^3}{y^5}-6r^2U_\infty\frac{x^5}{y^7}+8r^2U_\infty\frac{x^7}{y^9} \tag{6}$$

If the vertical wind velocity by Eq. (6) is set to be zero, following two coordinates can be obtained

$$\begin{cases} x_1 = -0.778y \\ x_2 = 0 \end{cases} \tag{7}$$

where x_1 and x_2 denote the x-coordinates for the start and end positions of the transition section, respectively. Substituting Eq. (7) into Eq. (5), the corresponding y-coordinates for these two positions can be expressed as

$$\begin{cases} y_1 - \dfrac{0.673r^2}{y_1} = \dfrac{\psi_5}{U_\infty} \\ y_2 - \dfrac{r^2}{y_2} = \dfrac{\psi_5}{U_\infty} \end{cases} \tag{8}$$

Further, the y-coordinates can be given by the following closed forms

$$\begin{cases} y_1 = \dfrac{m + \sqrt{m^2 + 2.692r^2}}{2} \\ y_2 = \dfrac{m + \sqrt{m^2 + 4r^2}}{2} \end{cases} \tag{9}$$

where $m = \psi_5/U_\infty$.

Hence, the start position (x_1, y_1) and the end position (x_2, y_2) on the transition section are determined by Eqs. (7) and (9), respectively. The second principle for an appropriate transition section addressed in introduction requires that the total flow transition length should be sufficiently short. In other words, the summation of the length of the transition section and that of the oncoming wind flowing from the end position of the transition section to the position where the wind field becomes stable and approaches to the undisturbed reference wind field should be as short as possible. Clearly, the shortest transition section (refer to the projected length) means that the equivalent slope k_0, shown in Fig. 5, must reach its maximum

$$k_0 = \frac{y_2 - y_1}{x_2 - x_1} = \frac{y_2 - y_1}{0.778y_1} \tag{10}$$

Substituting Eq. (9) into Eq. (10), the following equation can be derived

$$k_0 = 1.285\left(\frac{\sqrt{m^2 + 4r^2} - \sqrt{m^2 + 2.692r^2}}{m + \sqrt{m^2 + 2.692r^2}} \right) \tag{11}$$

By taking the limit on the right side of Eq. (11), i.e., $m \to -\infty$, k_0 achieves its maximum value, which is $k_{0\max} = 0.624$. Obviously, this maximum value is independent of the value of r. The height of the transition section is equal to that of the terrain model at edge, h_0, i.e., $h_0 = y_2 - y_1$. According to Eqs. (9) and (11), the relationship between the parameters r and m can be obtained as follows

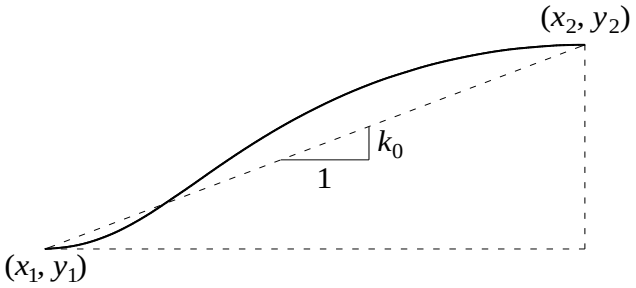

Fig. 5 Equivalent slope of the transition section curve

$$\begin{cases} \dfrac{m+\sqrt{m^2+4r^2}}{2}-\dfrac{m+\sqrt{m^2+2.692r^2}}{2}=h_0 \\ 1.285\left(\dfrac{\sqrt{m^2+4r^2}-\sqrt{m^2+2.692r^2}}{m+\sqrt{m^2+2.692r^2}}\right)=k_0 \end{cases} \tag{12}$$

Note that the above equations are all derived based on the theory of the potential flow, where the viscosity is neglected. Therefore, in the real viscous fluid, the value of k_0 should be adjusted. However, it must be smaller than $k_{0\max}$= 0.624. Clearly, the number of the series terms in Eqs. (5) and (6) can be increased or decreased according to the resolution requirement. When the values of h_0 and k_0 are determined, the values of r and m can be obtained by solving Eq. (12). By substituting r and m ($m = \psi_5/U_\infty$) into Eq. (5), the following form of the curved transition section can be derived

$$y-\frac{r^2}{y}+\frac{r^2x^2}{y^3}-\frac{r^2x^4}{y^5}+\frac{r^2x^6}{y^7}-\frac{r^2x^8}{y^9}-m=0 \tag{13}$$

3. Setup of wind tunnel test

To investigate the validity of the proposed curved transition section shown in Eq. (13), for the mountain-gorge terrain modeling, tests were conducted in the XNJD-1 wind tunnel of Southwest Jiaotong University. The test section of the wind tunnel is 2.4 m-wide, 2.0 m-high and 16.0 m-long, and the turbulence intensity of the empty tunnel is about 0.5% at the average wind velocity of 15.0 m/s. Considering that a transition section with a slope of 30° had previously been applied in practical engineering project (Hu *et al*. 2006), the curved transition section with an equivalent slope of 30° (referred to as 30° CTS) was adopted in the tests. Corresponding to this slope, the value of k_0 is 0.577, which is certainly smaller than $k_{0\max}$= 0.624. To better investigate the flow transition performance of the curved transition section, a simplified 2-D platform terrain model was used instead of a real 3-D complex terrain. Since the blockage ratio of a wind tunnel test is

generally smaller than 5%, the height of 2-D test model should be lower than 0.1 m. However, a terrain model with a height of 0.1m may be too small. On the one hand, a thick boundary layer produced by a long fetch of the oncoming wind could envelop the low terrain model to a large degree, and hence could result in large errors. On the other hand, it is also difficult to measure the wind velocity distribution for a low terrain model. Thus the height of the terrain model was finally decided to be 0.25 m. Meanwhile, to reduce the influence of the blockage effect of the wind tunnel, the flow transition performance of different transition sections and the normalized wind parameters were studied. Hence, no blockage corrections were made to the measurements in this study. Since the height of the terrain model is 0.25m, the height of the curved transition section h_0 should also equal to 0.25 m. From the given k_0 and h_0, the shape of the curved transition section with an equivalent slope of 30° can be determined by Eqs. (12) and (13), and it is given by the following equation

$$y-\frac{8.482}{y}+\frac{8.482x^2}{y^3}-\frac{8.482x^4}{y^5}+\frac{8.482x^6}{y^7}-\frac{8.482x^8}{y^9}+9.713=0 \quad (-0.433\le x\le 0) \tag{14}$$

Although the ramp transition section with the slope of 30° (referred to as 30° RTS) had been applied in the previous projects, it may be not an appropriate shape to serve as the boundary transition section as discussed in introduction. To make a comparison of flow transition performance between the curved transition section proposed in this paper and the ramp transition section, a test using 30° RTS was also conducted in the wind tunnel. According to existing research by numerical simulation methods (Hu *et al*. 2012) and related research by Kondo *et al*. (2002), the curved transition section with an equivalent slope of 10° (referred to as a 10° CTS) cannot result in an obvious speed-up or flow separation when the oncoming wind flows over it. As a result, the wind characteristics of the oncoming wind flowing over a 10° CTS can be well preserved; its shape is given by the following equation

$$y-\frac{2.213}{y}+\frac{2.213x^2}{y^3}-\frac{2.213x^4}{y^5}+\frac{2.213x^6}{y^7}-\frac{2.213x^8}{y^9}-1.003=0 \quad (-1.418\le x\le 0) \tag{15}$$

Because of the exceptional flow transition performance by 10° CTS, in this study, a 10° CTS will be used as the reference model in order to evaluate the flow transition performances of other models including 30° CTS and 30° RTS. The three different transition sections are shown in Fig. 6.

Fig. 7 shows the layout of the whole terrain model, together with the coordinate system utilized in this study, where *x'* and *y'* are the longitudinal and the vertical directions, respectively. The curved transition section or the ramp transition section was set in the front of the whole terrain, and the 2-D platform terrain was set behind the transition section. According to the second principle for determining an appropriate transition section, the length of the platform terrain should be long enough to make the wind field become stable, after the oncoming wind has flowed over the different transition sections. Based on the length of the test section of the wind tunnel and previous research by numerical simulation method (Hu *et al*. 2012), the length of the platform was finally determined to be 7.5 m. Furthermore, a ramp plate with a slope of 10° was set up at the end of the platform to allow the wind to flow away smoothly. In the tests, Cobra probes with a measurement precision of ±0.3 m/s were used to measure the wind velocity over the terrain. To obtain the average wind velocity, the sampling time was about 60s for each measurement position.

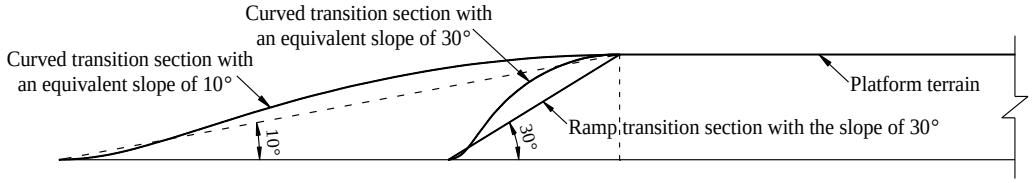

Fig. 6 Three different transition sections

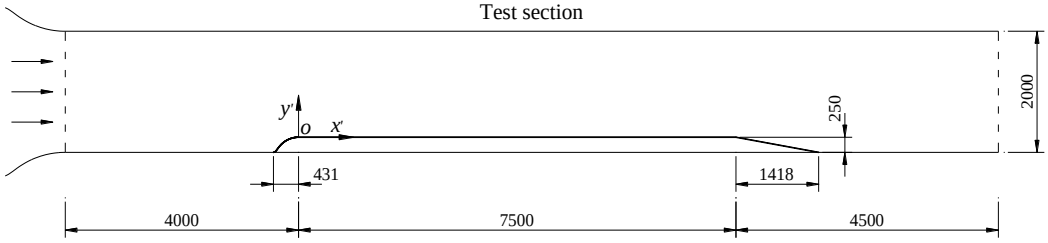

Fig. 7 Layout of the whole terrain model (Unit: mm)

4. Wind velocity field over platform terrain with ramp and curved transition sections

Uniform flow with the wind velocity of 15.0 m/s was selected in wind tunnel testing. The wind velocities along the platform at y' = 0.010 m and 0.290 m for the preceding three different transition sections are shown in Fig. 8. For the lower position at y' = 0.010 m, the wind velocities associated with the two curved transition sections decrease as the longitudinal positions move away from x' = 0.0 m (the position is the intersection between the transition section and the platform), and become almost constant after x' = 2.6 m. By comparison, the wind velocities along the platform for the 10° CTS are found to have less change than those for the 30° CTS, which indicates that the former has less influence on the wind characteristics of the oncoming wind. In the case of the 30° RTS, the wind velocities have a large variation around x' = 0.0m and also approach a constant value after x' = 2.6 m. The overall variation of wind velocities along the platform induced by the preceding three transition sections can be explained as follows. As the oncoming wind approaches the transition section, the wind velocity increases due to the smaller flow section. Then the oncoming wind flows over the platform terrain, and the wind velocity gradually becomes stable owing to the unchanged flow section. On the other hand, different transition sections will lead to different wind velocity fields. To be specific, when the approaching wind flows over the curved transition section, the wind pressure will change slightly and continuously along the curved transition section and the platform terrain, due to the smooth and continuous shape of the curved transition section. However, when the approaching wind flows over the ramp transition section, the wind pressure and velocity will undergo a noticeable variation along the ramp transition section and the platform terrain. The major reason can be attributed to that the ramp transition section is discontinuous at x' = 0.0 m (see position *s* in Fig. 3), resulting in a significant adverse pressure gradient and a very low wind velocity, and a possible flow

separation at this position (Bowen and Lindley 1977, Hu *et al*. 2012). For the higher position at *y'* = 0.290 m, the wind velocity field induced by the three different transition sections have similar features. These wind velocities decrease first and then become constant after a short distance. The reason is that the position *y'* = 0.290 m is in the potential flow region where the wind velocities mainly depend on the oncoming wind velocity rather than the three different transition sections.

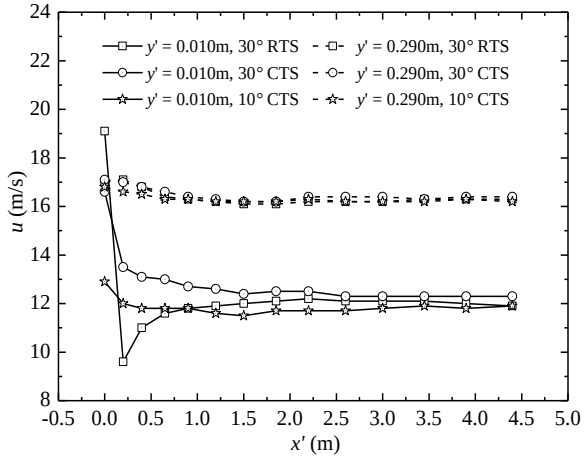

Fig. 8 Wind velocities along the platform at *y'* = 0.010 m and 0.290 m for different transition sections

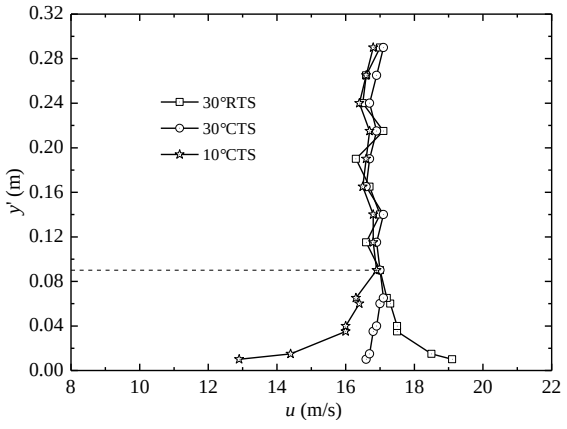

Fig. 9 Wind velocity profiles at *x'* = 0.0 m for different transition sections

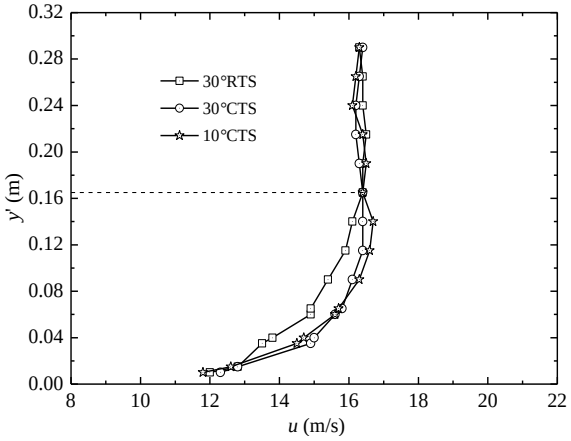

Fig. 10 Wind velocity profiles at *x'* = 3.9 m for different transition sections

Fig. 9 shows the wind velocity profiles at x' = 0.0 m induced by the three different transition sections. It can be observed that a significant speed-up behavior occurs near the wall in the wind velocity profile induced by the ramp transition section, while this speed-up behavior induced by the two curved transition sections are not so remarkable, especially for the 10° CTS. Also the wind velocity profile shape induced by the 30° CTS is closer to that induced by the 10° CTS. Fig. 10 shows the corresponding wind velocity profiles at x' = 3.9 m where the measurement positions are near the midline of the platform. The results show that the wind velocity profile shapes induced by the two curved transition sections are almost the same, but the wind velocities under y' = 0.165 m induced by the ramp transition section are obviously smaller than those induced by the two curved transition sections. The main reason for the variation of wind velocity profiles in Figs. 9 and 10 is that an obvious shear layer is developed, due to a significant adverse pressure gradient and a very low wind velocity around the position of x' = 0.0 m when the oncoming wind is flowing over the 30° RTS. Furthermore, the range of the shear layer increases with the oncoming wind flowing along the platform, and when the oncoming wind reaches the position of x' = 3.9 m, the shear layer becomes thicker and makes the wind velocities in its range smaller than those outside its range. Also, similar behavior was noted in wind tunnel tests described by Bowen and Lindley (1977). However, because of the smooth and continuous shape of the curved transition section, as discussed previously, the shear layers at x' = 3.9 m induced by the oncoming wind flowing over the two curved transition sections are relatively thin, which have little influence on the wind velocities along the platform. As a result, the wind velocities at x' = 3.9 m induced by these two curved transition sections are almost the same and the corresponding wind velocities under y' = 0.165 m are larger than those induced by the ramp transition section. Overall, compared with the wind velocity field induced by the 30° RTS, the wind velocity field induced by the 30° CTS is closer to that induced by 10° CTS which has the best flow transition performance in maintaining the characteristics of the approaching wind flow.

As discussed previously, because the 10° CTS has best flow transition performance, and the wind field over the platform terrain induced by the 10° CTS can be used as the reference. To further analyze the differences of wind field induced by the 30° CTS and the 30° RTS, a parameter called 'average velocity ratio' can be defined based on the wind field induced by the 10° CTS, which is given by

$$a(x', y') = \frac{1}{N} \sum_{y'>0}^{H} \frac{\left| u(x', y') - u_0(x', y') \right|}{u_0(x', y')} \tag{16}$$

where H is the average height of the shear layer of the three different transition sections. For example, at x' = 0.0 m, the average height of the shear layer is about 0.09 m (shown in Fig. 9), and at x' = 3.9 m, it is about 0.165 m (shown in Fig. 10); $u(x', y')$ is the wind velocity at the measurement position (x', y') for different transition sections; $u_0(x', y')$ is the wind velocity at the measurement position (x', y') for 10° CTS; N is the number of the measurement positions between the platform surface and the average height of the shear layer. Therefore, smaller values of $a(x', y')$ means the wind field over the platform terrain induced by a transition section is closer to that induced by the 10° CTS.

Fig. 11 shows $a(x', y')$ along the platform for the 30° RTS and 30° CTS. It can be observed that the values of $a(x', y')$ for the ramp transition section case are significantly larger than those of the curved transition section case, which indicates the 30° CTS has a better performance in retaining the wind characteristics of oncoming wind.

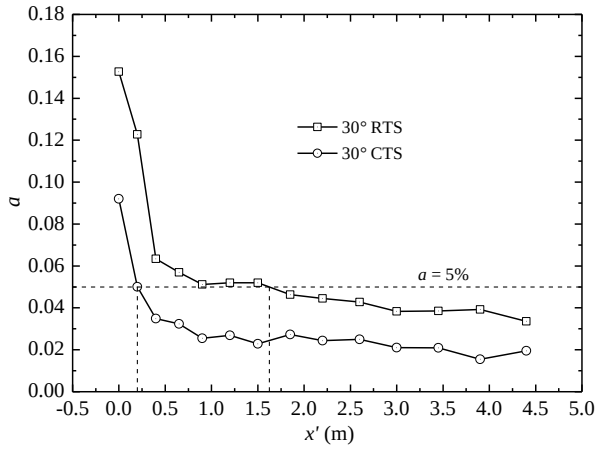

Fig. 11 Average velocity ratio $a(x', y')$ along the platform with curved and ramp transition sections

Furthermore, it can be seen from Fig. 11 that for a given value of $a(x', y')$, the curved transition section leads to a much smaller x' than the ramp transition section. Specifically, take $a(x', y')$ equal to 5% as an example, the corresponding values of x' for the curved and the ramp transition sections are about 0.2 m and 1.6 m, respectively, i.e., x' associated with the latter is noticeably larger than that associated with the former. This comparison indicates that the oncoming wind flowing over the 30° CTS can reach stability earlier than that of the 30° RTS. Similar results can be obtained for other smaller $a(x', y')$. Note that although both transition sections have a slope of 30°, the curved transition section has a shorter total flow transition length than the ramp transition section. Based on the two principles for selecting an appropriate shape of boundary transition section presented in introduction, the 30° CTS is more appropriate to provide a boundary transition section for the mountain-gorge terrain model than the 30° RTS.

5. Stability analysis of wind velocity field

Since the 30° CTS is more appropriate to served as the boundary transition section, it will be further investigated in this section. To better describe the wind field induced by this transition section, a parameter called ‘velocity stability factor’ is defined. The effects of some factors such as the oncoming wind velocity (denoted by U) and terrain model height (denoted by h) on the velocity stability factor are studied. Furthermore, an analytical model to predict the velocity stability factor is proposed.

5.1 Effects of oncoming wind velocity and terrain height

To investigate the effects of oncoming wind velocity on the wind velocity field over the platform, the tests with the oncoming wind velocities of 10.1 m/s, 15.0 m/s and 19.6 m/s were

carried out. To better compare the effects of different oncoming wind velocities, wind velocities over the platform were normalized by the corresponding oncoming wind velocity. The normalized wind velocities, denoted by $n(x', y')$, along the platform at y' = 0.010 m and 0.290 m and the normalized wind velocity profiles at x' = 0.0 m and 3.9 m are shown in Figs. 12 and 13, respectively, where the normalized wind velocities and profiles are almost the same for different oncoming wind velocities. Moreover, the normalized wind velocities in Fig. 12 generally monotonically decrease with the increase of x' and gradually become stable. Also, similar wind velocity variation can be found in Fig. 8 for both the curved transition sections.

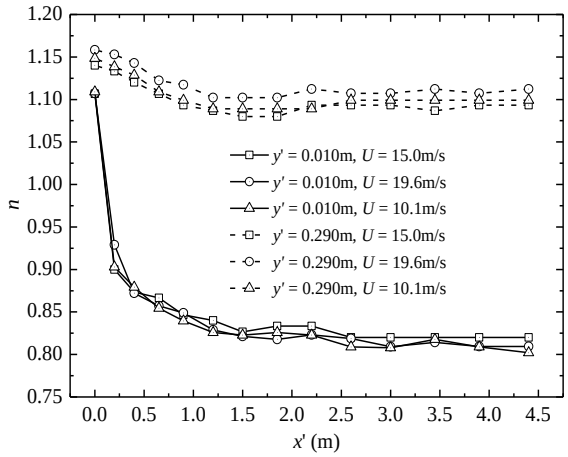

Fig. 12 Normalized wind velocities $n(x', y')$ along the platform at y' = 0.010 m and 0.290 m

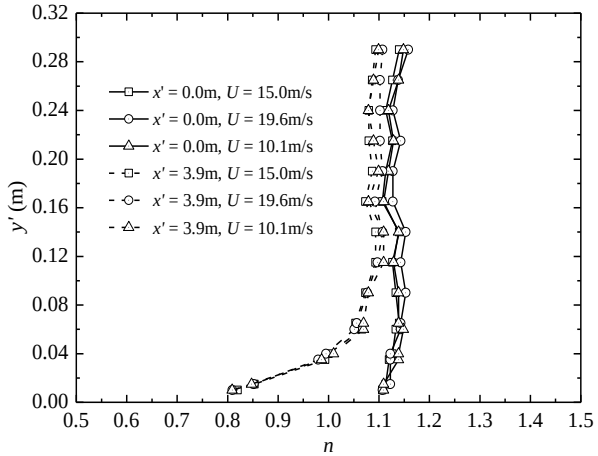

Fig. 13 Normalized wind velocity profiles at x' = 0.0 m and 3.9 m

In order to measure whether the wind field can become stable, a new parameter called 'velocity stability factor' $s(x', y')$ is defined as

$$s(x', y') = \frac{u(x', y') - u(x'_{\infty}, y')}{u(x'_{\infty}, y')} \tag{17}$$

where $u(x'_{\infty}, y')$ is the wind velocity at the longitudinal position very far away from $x = 0.0$ m. In the present study, the wind velocities at the positions close to $x' = 3.9$ m, where the wind velocities have already become stable, shown in Figs. 8 and 12, are averaged and used for calculating the value of $u(x'_{\infty}, y')$. Obviously, the value of $s(x', y')$ will monotonically decrease to zero with the increase of x'. Therefore, $s(x', y')$ can be used to judge whether the wind field induced by the curved transition section has become stable.

From Fig. 9, it can be seen that the wind field is not stable yet at $x' = 0.0$ m. Therefore, there exists a noticeable difference between the wind velocity profiles induced by the 30° CTS and 10° CTS. On the other hand, at $x' = 3.9$ m shown in Fig. 10, the wind field is almost stable. Hence, the wind velocity profiles induced by these two curved transition sections are almost the same. As discussed previously, the 10° CTS produces the least disturbance on the oncoming wind field, and the characteristics of the wind field induced by the 10° CTS are the closest to those of the oncoming wind. Therefore, if the wind field induced by the 30° CTS becomes stable, its wind characteristics in that case are also very close to those of the oncoming wind field. From the above, it can be seen that the velocity stability factor $s(x', y')$ not only can judge whether the wind field induced by the curved transition section has become stable, but also can evaluate how close to the oncoming wind field for the wind field induced by the curved transition section. Hence, it can be concluded that the velocity stability factor $s(x', y')$ can be used to analyze the flow transition performance of different curved transition sections.

Note that the relationship between the normalized wind velocities $n(x', y')$ and the velocity stability factor $s(x', y')$ are given as Eq. (18). It is seen that the values of $s(x', y')$ can be determined by the values of $n(x', y')$. From the Figs. 12 and 13, the values of $n(x', y')$ are almost independent of the oncoming wind velocity at the given x' and y'. Then it can be concluded from Eq. (18) that the values of $s(x', y')$ are also independent of the oncoming wind velocity. To validate this observation, the velocity stability factor $s(x', y')$ at some vertical positions such as $y' = 0.010$ m, 0.015 m and 0.035 m with different oncoming wind velocities are calculated and shown in Fig. 14. For a given vertical position y', the values of $s(x', y')$ may vary with the different oncoming wind velocities, but the variation are rather limited. For the vertical positions at $y' = 0.010$ m and 0.015 m, the differences for $s(x', y')$ induced by the different vertical positions are significantly larger than those induced by the different oncoming wind velocities. Therefore, it can be concluded that $s(x', y')$ is more sensitive to the measurement positions (x', y') than the oncoming wind velocities, which validates the preceding observation. Moreover, when the values of x' or y' increase, the values of $s(x', y')$ generally decrease, indicating that the wind field is becoming stable and approaching to the undisturbed reference wind field with the increase of x' or y'.

$$\begin{aligned} s(x', y') &= \frac{u(x', y')/U}{u(x'_{\infty}, y')/U} - 1 \\ &= \frac{n(x', y')}{n(x'_{\infty}, y')} - 1 \end{aligned} \tag{18}$$

To further investigate the effects of terrain model heights on the values of $s(x', y')$, tests of two other terrain models with heights of 0.20 m and 0.15 m were conducted. In these two terrain models, the equivalent slope of the curved transition section, the length of the platform and the slope of the ramp plate at the end were the same as before. The only difference was that the heights of the three parts were changed from 0.25 m to 0.20 m and 0.15 m, respectively. The corresponding values of $s(x', y')$ with different terrain model heights are shown in Fig. 15, where the variation of $s(x', y')$ are almost identical to those in Fig. 14. More importantly, the differences of the values of $s(x', y')$ induced by the different measurement positions (x', y') are still generally significantly larger than those induced by the different terrain model heights. Similarly, the values of $s(x', y')$ are more sensitive to the measurement positions (x', y') than the heights of the terrain model. Moreover, it also can be seen from Fig. 15 that the values of $s(x', y')$ all generally decrease with the increase of x' or y'. Hence, the wind field is also becoming stable and approaching to the undisturbed reference wind field with increasing x' or y'.

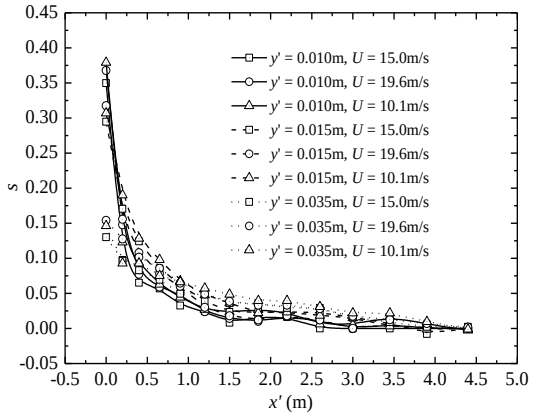

Fig. 14 Distributing of velocity stability factor $s(x', y')$ with different oncoming wind velocities

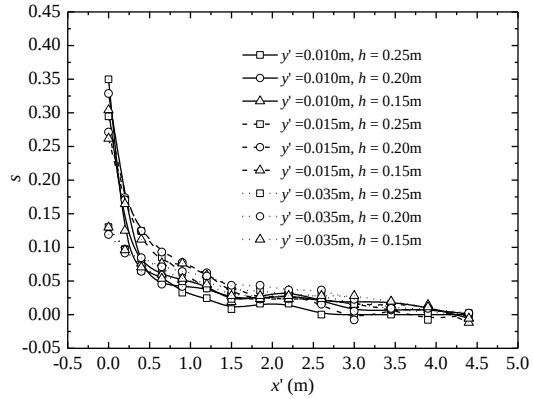

Fig. 15 Distributing of velocity stability factor $s(x', y')$ with different terrain model heights

5.2 Analytical model for predicting s(x', y') based on potential flow theory around a blunt nosed semi-infinite streamline body

As discussed previously, $s(x', y')$ can be an effective parameter to analyze the flow transition performance of the curved transition section. To evaluate the wind field induced by the 30° CTS more conveniently and directly in engineering practice, an analytical model to predicate $s(x', y')$ is proposed, based on potential flow theory around a blunt nosed semi-infinite streamline body and the corresponding test data.

5.2.1 Potential flow theory around a blunt nosed semi-infinite streamline body

As a uniform rectilinear potential flow passes a particle source flow, the corresponding stream function and wind velocities are given as follows (Kundu and Cohen 2008)

$$\psi_0 = U_\infty r \sin\theta + \frac{q}{2\pi}\theta \tag{19}$$

$$u_r = \frac{1}{r}\frac{\partial \psi_0}{\partial \theta} = U_\infty \cos\theta + \frac{q}{2\pi r} \tag{20}$$

$$u_\theta = -\frac{\partial \psi_0}{\partial r} = -U_\infty \sin\theta \tag{21}$$

where q is the flux per unit length of the particle source flow; r and θ are the corresponding polar coordinates of the flow field, as shown in Fig. 16. From Eqs. (19)-(21), the coordinate values of the stagnation point P are $r_P = q/2\pi U_\infty$ and $\theta_P = \pi$.

As discussed previously, each streamline can be regarded as a wall with no influences on the oncoming wind movements. For the unique shape of the streamline passing through the stagnation point P (shown in Fig. 16), regarding this streamline as a wall, then this type of flow field is termed as the potential flow around a blunt nosed semi-infinite streamline body, or potential flow passing a half-body (Kundu and Cohen 2008).

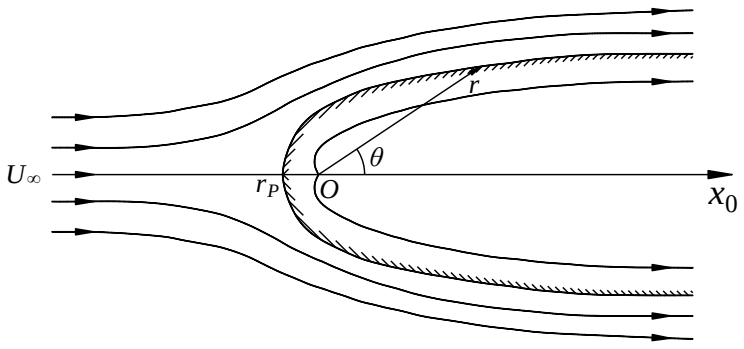

Fig. 16 Potential flow around a blunt nosed semi-infinite streamline body

5.2.2 Analytical model for predicting s(x', y') for curved transition section with equivalent slope of 30°

For the terrain model in Fig. 7, the 30° CTS can be regarded as a blunt body. Because the length of the platform is over 16 times longer than that of this curved transition section, the platform is regarded as a semi-infinite streamline body compared with this small curved transition section, and the whole terrain model can be considered as a blunt nosed semi-infinite streamline body. Accordingly, some wind characteristics over this curved transition section may be similar to those of the potential flow around the blunt nosed semi-infinite streamline body introduced in section 5.2.1. In order to develop the expression form of the velocity stability factor, Eq. (20) can be converted to rectangular coordinates from polar coordinates, given by

$$u_0 = \frac{\partial \psi_0}{\partial y_0} = U_\infty + \frac{q}{2\pi} \cdot \frac{x_0}{x_0^2 + y_0^2} \tag{22}$$

where u_0 is the longitudinal velocity in the corresponding rectangular coordinate; x_0 and y_0 are the corresponding rectangular coordinates in the flow field. According to Eq. (17), the velocity stability factor for the potential flow around the blunt nosed semi-infinite streamline body is given as

$$\begin{aligned} s(x_0, y_0) &= \frac{q}{2\pi U_\infty} \cdot \frac{1}{x_0 + y_0^2 / x_0} \\ &= r_P \cdot \frac{1}{x_0 + y_0^2 / x_0} \end{aligned} \tag{23}$$

The characteristics of wind flows over the 30° CTS and the platform terrain are similar to those of the potential flow around the blunt nosed semi-infinite streamline body to a certain degree. Therefore, it can be assumed that the velocity stability factor $s(x', y')$ of the 30° CTS also has a similar form as the velocity stability factor $s(x_0, y_0)$ of Eq. (23). On the other hand, there exist some difference in shape between the whole terrain in Fig. 7 and the blunt nosed semi-infinite streamline body in Fig. 16. Besides, the wind in the tests is a real viscous fluid, and it cannot in reality be regarded as potential flow, meaning that $s(x_0, y_0)$ cannot be used directly. Hence, Eq. (23) should be modified.

For Eq. (23), $s(x_0, y_0)$ is related to the distance from the stagnation point P to the origin point O, r_P (shown in Fig. 16), which implies that $s(x_0, y_0)$ is relevant to the shape of the blunt nosed semi-infinite streamline body. On the other hand, the variation range for y' is much smaller than that for x' (shown in Fig. 7). Therefore, the term y_0^2/x_0 in Eq. (23) can be neglected for the present tests. Furthermore, noting the discussion in Section 5.1, the values of $s(x', y')$ vary little with the oncoming wind velocity or the terrain model height, but are very sensitive to the measurement position (x', y'). From the above, the form of the velocity stability factor $s(x', y')$ can be approximately expressed as

$$s(x', y') = \frac{f_1(y')}{x' + f_2(y')} \tag{24}$$

where $f_1(y')$ and $f_2(y')$ are both the function of y'. Compared with the Eq. (23), the term $f_1(y')$ is to consider the difference in shape between the terrain model in the tests and the blunt nosed semi-infinite streamline body, and the term $f_2(y')$ is to consider the effects of neglecting the term y_0^2/x_0 in Eq. (24).

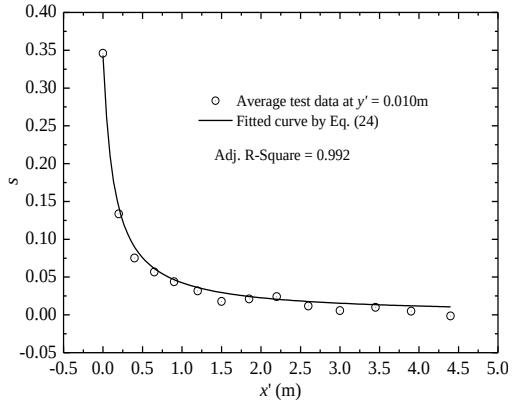

(a) y'= 0.010m

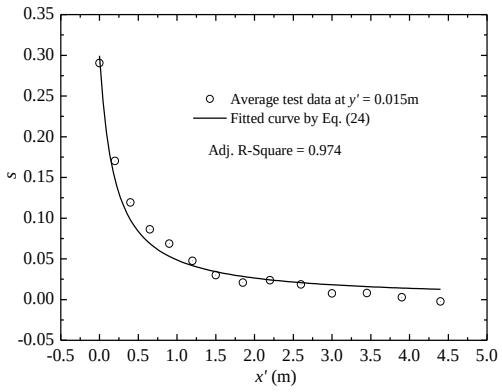

(b) y'= 0.015m

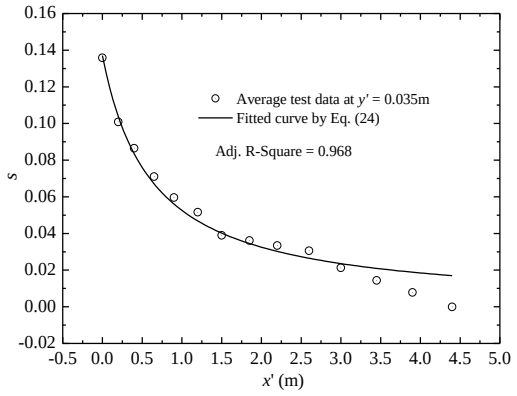

(c) y'= 0.035m

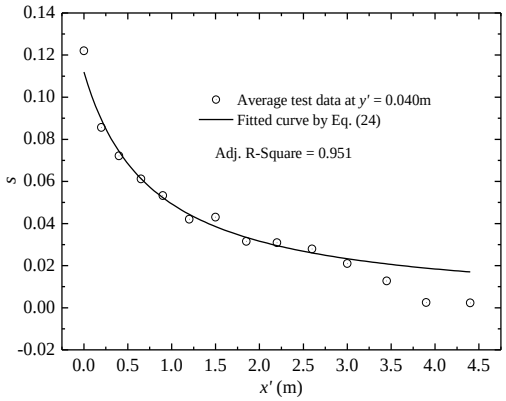

(d) y'= 0.040m

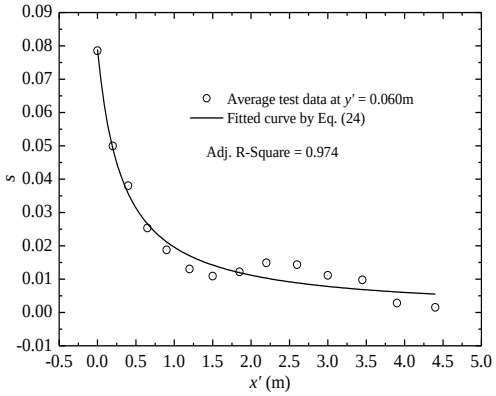

(e) y'= 0.060m

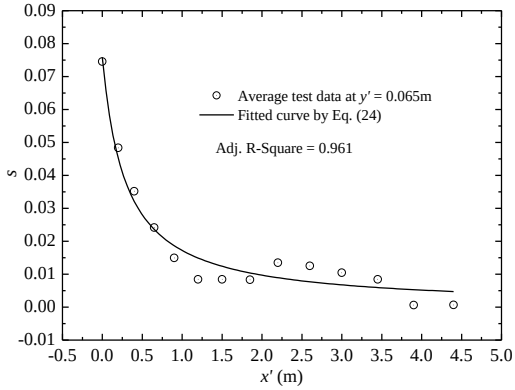

(f) y'= 0.065m

Fig. 17 Fitted results of velocity stability factor $s(x', y')$ at different vertical heights

To verify the accuracy of Eq. (24) in predicting $s(x', y')$, for different y', Eq. (24) was fitted to the average test values of $s(x', y')$ for the different oncoming wind velocities and different terrain heights. The six sets of fitted results of $s(x', y')$, which all have relatively large values, are shown in Fig. 17. Note the fitted parameter Adj.R-Square (OriginLab Corporation 2010) are all larger than 0.95, which indicates that Eq. (24) is accurate. Accordingly, for each value of y', a set of values for $f_1(y')$ and $f_2(y')$ can be obtained. The corresponding six sets of $f_1(y')$ and $f_2(y')$ values are shown in Figs. 18 and 19. It can be seen that $f_1(y')$ and $f_2(y')$ can be divided into two parts, the first four sets of $f_1(y')$ and $f_2(y')$ approximately increase linearly with y', but the last two sets of $f_1(y')$ and $f_2(y')$ are irregular. The reason could be that the last two sets of values of $s(x', y')$ are much smaller than the first four sets of values of $s(x', y')$, resulting in a relatively large error when fit Eq. (24) to the test data. As a result, the corresponding values of $f_1(y')$ and $f_2(y')$ also have a relatively large errors. Furthermore, it is noted in wind engineering, attention is focused on wind characteristics near the ground. Therefore, the first four sets of $f_1(y')$ and $f_2(y')$ values should clearly be investigated in the present study. By the linear fitting method, these are given as: $f_1(y') = 1.366y' + 0.037$ and $f_2(y') = 21.512y' - 0.102$, respectively. It can be seen, from Figs. 18 and 19 that the fitting is accurate because the values of Adj.R-Square are all larger than 0.98.

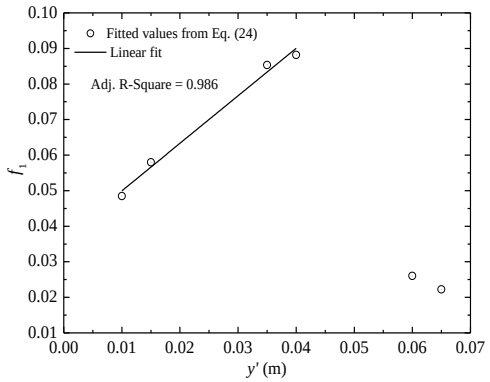

Fig. 18 Fitted results of $f_1(y')$

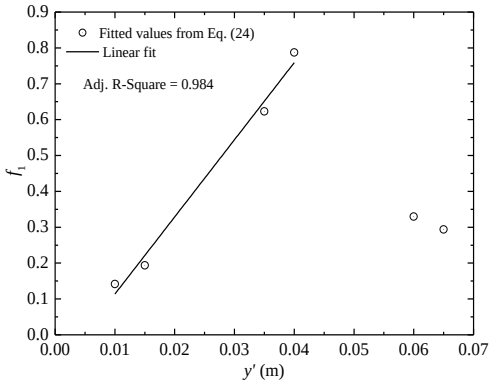

Fig. 19 Fitted results of $f_2(y')$

6. Conclusions

To determine the appropriate shape of boundary transition section for the mountain-gorge terrain model, two principles for selecting its appropriate shape were proposed, a type of theoretical curves serving as its shape was derived, and the corresponding wind tunnel tests were conducted. The main conclusions are summarized as follows:

- A type of theoretical curve was developed based on the potential flow theory around a circular cylinder, and this type of curve could be used as the appropriate shape of boundary transition section for a mountain-gorge terrain model.
- Compared with the ramp transition section with the slope of 30°, the curved transition section with the equivalent slope of 30° can better maintain the wind characteristics of the reference oncoming wind field. Furthermore, the total flow transition length of the wind field for a curved transition section is shorter than that for the ramp transition section. Therefore, a curved transition section with the equivalent slope of 30° can be more appropriate to serve as the boundary transition section for the mountain-gorge terrain model than the ramp transition section with the slope of 30°.
- The 'velocity stability factor' was defined to describe the stability of the wind field induced by the curved transition section with the equivalent slope of 30°, and it was found that the oncoming wind velocity and the terrain model height had no significant influence on this factor. Furthermore, an analytical model for predicting the velocity stability factor was proposed, based on potential flow theory around a blunt nosed semi-infinite streamline body and the corresponding test data.

Acknowledgements

This work was financially supported by the National Natural Science Foundation of China under Grant NNSF-51408496, 90915006 and U1334201. The authors also sincerely thank Dr. Xinzhong Chen at the Texas Tech University for his encouraging comments.

References

Bowen, A.J. (2003), "Modelling of strong wind flows over complex terrain at small geometric scales", *J. Wind Eng. Ind. Aerod.*, **91**(12-15), 1859-1871.

Bowen, A.J. and Lindley, D. (1977), "A wind-tunnel investigation of the wind speed and turbulence characteristics close to the ground over various escarpment shapes", *Bound. – Lay. Meteorol.*, **12**(3), 259-271.

Cao, S. and Tamura, T. (2006), "Experimental study on roughness effects on turbulent boundary layer flow over a two-dimensional steep hill", *J. Wind Eng. Ind. Aerod.*, **94**(1), 1-19.

Carpenter, P. and Locke, N. (1999), "Investigation of wind speeds over multiple two-dimensional hills", *J. Wind Eng. Ind. Aerod.*, **83**(1-3), 109-120.

Cermak, J.E. (1984), "Physical modelling of flow and dispersion over complex terrain", *Bound. – Lay. Meteorol.*, **30**(1-4), 261-292.

Chock, G.Y.K. and Cochran, L. (2005), "Modeling of topographic wind speed effects in Hawaii", *J. Wind Eng. Ind. Aerod.*, **93**(8), 623-638.

Currie, I.G. (2003), *Fundamental Mechanics of Fluids*, (3th Ed.), CRC Press, Boca Raton, Florida, USA.

Derickson, R.G. and Peterka, J.A. (2004), "Development of a powerful hybrid tool for evaluating wind power in complex terrain: atmospheric numerical models and wind tunnels", *Proceedings of the 23rd ASME Wind Energy Symposium*, Reno, Nevada, USA, January.

Hu, F.Q., Chen, A.R. and Wang D.L. (2006), "Experimental study of wind field in bridge site located in mountainous area", *J. Tongji Univ. Natural Sci.*, **34**(6), 721-725 (in Chinese).

Hu, P., Li, Y.L. and Liao, H.L. (2012), "Appropriate shape of boundary transition section of terrain model for mountains-gorge bridge site", *Proceedings of the 7th International Colloquium on Bluff Body Aerodynamics and Applications*, Shanghai, China, September.

Hui, M.C.H., Larsen, A. and Xiang, H.F. (2009), "Wind turbulence characteristics study at the Stonecutters Bridge site: Part I—Mean wind and turbulence intensities", *J. Wind Eng. Ind. Aerod.*, **97**(1), 22-36.

Hunt, J.C.R., Leibovich, S. and Richards, K.J. (1988), "Turbulent shear flow over low hills", *Q. J. Roy. Meteorol. Soc.*, **114**(484), 1435-1470.

Iizuka, S. and Kondo, H. (2004), "Performance of various sub-grid scale models in large-eddy simulations of turbulent flow over complex terrain", *Atmos. Environ.*, **38**(40), 7083-7091.

Jackson, P.S. and Hunt, J.C.R. (1975), "Turbulent wind flow over a low hill", *Q. J. Roy. Meteorol. Soc.*, **101**(430), 929-955.

Kim, H.G., Patel, V.C. and Lee C.M. (2000), "Numerical simulation of wind flow over hilly terrain", *J. Wind Eng. Ind. Aerod.*, **87**(1), 45-60.

Kondo, K., Tsuchiya, M. and Sanada, S. (2002), "Evaluation of effect of micro-topography on design wind velocity", *J. Wind Eng. Ind. Aerod.*, **90**(12-15), 1707-1718.

Kundu, P.K. and Cohen, I.M. (2008), *Fluid Mechanics*, (4th Ed.), Academic Press, Burlington, Massachusetts, USA.

Li, C.G., Chen, Z.Q., Zhang, Z.T. and Cheung, J.C.K. (2010a), "Wind tunnel modeling of flow over mountainous valley terrain", *Wind Struct.*, **13**(3), 275-292.

Li, L., Zhang, L.J., Zhang, N., Hu, F., Jiang, Y., Xuan, C.Y. and Jiang, W.M. (2010b), "Study on the micro-scale simulation of wind field over complex terrain by RAMS/FLUENT modeling system", *Wind Struct.*, **13**(6), 519-528.

Loureiro, J.B.R., Alho, A.T.P. and Silva Freire, A.P. (2008), "The numerical computation of near-wall turbulent flow over a steep hill", *J. Wind Eng. Ind. Aerod.*, **96**(5), 540-561.

Mason, P. and Sykes, R. (1979), "Flow over an isolated hill of moderate slope", *Q. J. Roy. Meteorol. Soc.*, **105**(444), 383-395.

Maurizi, A., Palma, J.M.L.M. and Castro F.A. (1998), "Numerical simulation of the atmospheric flow in a mountainous region of the North of Portugal", *J. Wind Eng. Ind. Aerod.*, **74-76**, 219-228.

Meroney, R.N. (1980), "Wind-tunnel simulation of the flow over hills and complex terrain", *J. Wind Eng. Ind. Aerod.*, **5**(3-4), 297-321.

Neal, D., Stevenson, D.C. and Lindley, D. (1981), "A wind tunnel boundary-layer simulation of wind flow over complex terrain: Effect of terrain and model construction", *Bound. – Lay. Meteorol.*, **21**(3), 271-293.

OriginLab Corporation. (2010), *Origin Reference for Origin 8.5 SR1*, Northampton, Massachusetts, USA.

Tsang, C.F., Kwok, K.C.S., Hitchcock, P.A. and Hui, D.K.K. (2009), "Large eddy simulation and wind tunnel study of an uphill slope in a complex terrain", *Wind Struct.*, **12**(3), 219-237.

JH